International Journal of Mechanical and Electrical Engineering
ISSN: 3005-9615 (Print), ISSN: 3005-7132 (Online) | Volume 2, Number 3, Year 2024
DOI: https://doi.org/10.62051/ijmee.v2n3.03
Journal homepage: https://wepub.org/index.php/IJMEE/index

Analysis and Optimization Design of a New Structure U-shaped Permanent Magnet Linear Synchronous Motor

Lei Zhao *, Longqi Zhang, Shihao Li

School of Electrical Engineering and Automation, Henan Polytechnic University, Jiaozuo Henan, China

* Corresponding Author: Lei Zhao (Email: 286648541@qq.com)

ABSTRACT

A new structure of U-shaped permanent magnet synchronous linear motor is proposed to address the issue of low thrust in U-shaped coreless permanent magnet synchronous linear motors. The motor increased the electromagnetic thrust by 74.36% and controlled the thrust fluctuation within a small range by adding magnetic blocks in the primary and changing the main magnetic circuit structure. In the article, the permanent magnetic field in the motor air gap is first solved using analytical methods, and the influence of harmonic components on the motor thrust and thrust fluctuation is discussed through harmonic analysis of the magnetic flux density in the air gap. Then, the influence of several parameters on motor performance was analyzed, and the Taguchi method was used to screen the optimization variables. A mathematical model reflecting the functional relationship between optimization objectives and parameters was obtained through the response surface method. Finally, the multi-objective optimization algorithm of egret swarm was used to optimize the design of the motor and obtain the Pareto frontier. The effectiveness of the theoretical analysis was verified through finite element simulation.

KEYWORDS

U-type Permanent Magnet Synchronous Linear Motor; Magnetic Block; Magnetic Field Analysis; Multi-objective Optimization Design.

1. INTRODUCTION

Compared with rotary motors, linear motors have the advantages of simple structure, easy heat dissipation, high control accuracy and fast response speed, etc. In recent years, they have received more attention and have been applied more and more, and play an important role in some high-precision CNC machine tools [1-2]. However, the iron core linear motor reduces the stability of the motion system due to the effect of end force and notch force. It inhibits the application of linear motors to a certain extent. In contrast, bilateral permanent magnet synchronous linear motors [3-4] have the advantages of simple control and small normal force, which have received extensive attention from scholars at home and abroad.

Currently, the research for bilateral permanent magnet synchronous linear motors mainly focuses on two aspects: permanent magnet arrays and operating tracks. The former is used to increase the permanent magnet utilization and improve the air gap flux density magnitude by using different Halbach arrays. For example, literature [5] proposes an ironless core permanent magnet linear synchronous motor with Halbach structure for permanent magnets, which improves the air gap flux density distribution, sinusoidalizes the air gap flux density, improves the fundamental wave amplitude, and has a high acceleration performance in a high precision control system. Literature [6] changed

the rectangular Halbach permanent magnet array, to trapezoidal Halbach structure, which reduced the installation difficulty and magnetic field distortion rate of Halbach permanent magnet array. The air-gap magnetic flux density amplitude was further improved. The new structure permanent magnet array can effectively suppress the thrust fluctuation without weakening the motor thrust. Literature [7] permanent magnets are fixed using non-equally spaced assembly of Halbach permanent magnet arrays; it produces higher magnetic density at the same pole pitch and improves the motor thrust. Literature [8] investigated a trapezoidal Halbach alternating-pole permanent magnet array, which reduces the inter-pole leakage and the amount of permanent magnets, improves the utilization of permanent magnets, and reduces the thrust fluctuation.

At present, some foreign scholars propose a new track structure [9], which is used to reduce the amount of permanent magnets and increase the thrust density. Aiming at the influence of permanent magnets on the performance of the motor, the iron rail and permanent magnet track are matched with each other, and the performance is compared with the U-type ironless core permanent magnet synchronous linear motor. The results show that the new track structure of the linear permanent magnet motor has great potential for application in high-precision machine tools. In addition, linear motors have been widely used in the fields of miniature ultrasonic motors and magnetic levitation trains [10-13]. However, due to the poor magnetizing ability and low thrust density of U-type coreless linear motors, they are less used in some high-output and low-cost applications. Therefore, the research of U-type ironless core linear motors in improving the magnetizing ability and optimizing the thrust fluctuation is of great practical significance.

Aiming at the above problems, this paper proposes a new structure of U-type permanent magnet linear synchronous motor, which improves the magnetizing ability and thrust density by adding a magnetic guide block in the primary, and has the characteristics of small normal force and flexible control. On the premise of not much increase in cost and thrust fluctuation, it improves the motor output and provides a new program for high-precision linear motor design.

2. MOTOR STRUCTURE

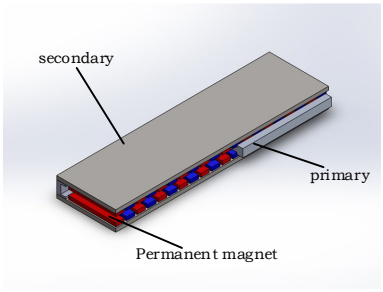

(a)three-dimensional model

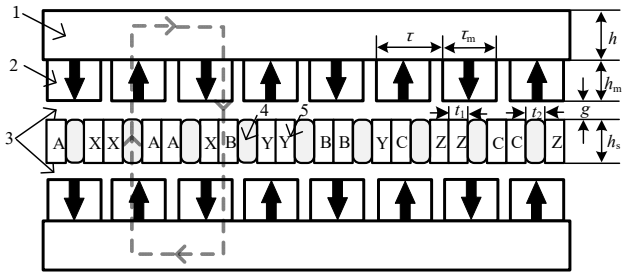

1--Secondary back iron 2--Permanent magnet 3--Air gap

4--Magnetic block 5--Primary winding

(b)2D structural diagram

Figure 1. New Structure U-shaped Permanent Magnet Synchronous Linear Moto

The structure of the new structure U-type permanent magnet linear synchronous motor is shown in Fig. 1, which is mainly composed of primary and secondary. The primary part consists of windings and magnetizing blocks, which are encapsulated with epoxy resin; the secondary is a double-sided structure, with each side consisting of a permanent magnet and a backing iron (yoke), and the secondary is in the shape of a "U". The magnetization direction of the permanent magnet poles and the path of the main magnetic flux are shown in Figure 1(b). The magnetizing block in the middle of the coil is made of ferromagnetic material, which has good magnetic conductivity, reduces the reluctance of the main magnetic circuit, enhances the main magnetic field of the air gap, and increases the output power of the motor.

3. AIR GAP PERMANENT MAGNETIC FIELD ANALYSIS

3.1. Permanent Magnetic Potential

The prototype analyzed in this paper consists of unit motors, each unit motor is 8 poles and 9 slots with fractional slot centralized winding, the structure is shown in Fig. 1. the parameters are shown in Table 1.

Table 1. Initial parameters of a new U-shaped permanent magnet synchronous linear motor structure

parameters	numerical value
coil edge width t_1/mm	5.5
coil edge height h_s/mm	7.21
width of magnetic guide block t_2/mm	5
unit primary length l/mm	144
polar distance τ/mm	18
current density J/A·mm^{-2}	6
secondary back-iron heights h/mm	10
Unilateral air gap length g/mm	0.84
Motor width d/mm	50
Permanent magnet magnetization height h_m/mm	6

To simplify the analytical analysis, the following reasonable assumptions are made:

(1) The permeability of the secondary yoke is infinite;

(2) The nonlinear effect of the material is not considered;

(3) The relative permeability of the permanent magnet is taken as 1;

(4) The motor extends infinitely along the x-axis direction (longitudinal direction, i.e., direction of motion), ignoring longitudinal end effects.

The motor has symmetry, and in order to simplify the analysis, only the upper part of the motor is solved. According to the arrangement of the upper permanent magnets, the distribution of the magnetic potential generated by them can be obtained as in Fig. 2.

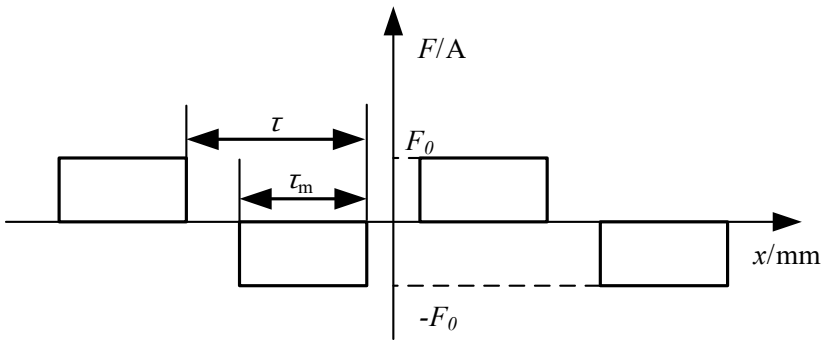

Figure 2. Distribution of permanent magnet pole magnetic potential

From Fig. 2, the distribution function of the magnetic potential of the permanent magnetic poles can be obtained as

$$F(x)=\begin{cases} 0 & k\tau-\dfrac{\tau-\tau_{\mathrm{m}}}{2}\le x\le k\tau+\dfrac{\tau-\tau_{\mathrm{m}}}{2} \\ (-1)^{k}F_{0} & k\tau+\dfrac{\tau-\tau_{\mathrm{m}}}{2}\le x\le k\tau+\dfrac{\tau+\tau_{\mathrm{m}}}{2} \end{cases} \tag{1}$$

$$F_{0}=\mathrm{H_c}h_{\mathrm{m}} \tag{2}$$

where $\mathrm{H_c}$ is the coercivity of the permanent magnet,h_{m} is the magnetization height of the permanent magnet, k=0, ±1, ±2,....

The Fourier series expansion of the magnetic potential distribution function of the permanent magnet is obtained:

$$F(x)=\sum_{k=1}^{\infty}\left(b_{k}\sin\frac{k\pi x}{l}\right) \tag{3}$$

Which

$$b_{k}=\frac{2}{l}\int_{0}^{l}F(x)\sin\frac{k\pi x}{l}\mathrm{d}x \tag{4}$$

Substituting (1) into (4) yields

$$b_{k}=\frac{(-1)^{k}4F_{0}}{k\pi}\sin\frac{(2k+1)k\pi\tau}{2l}\sin\frac{k\pi\tau_{\mathrm{m}}}{2l} \tag{5}$$

Organizing is available:

$$F(x)=\sum_{k=1}^{\infty}\frac{(-1)^{k}4F_{0}}{k\pi}\sin\frac{k\pi x}{l}\sin\frac{(2k+1)k\pi\tau}{2l}\sin\frac{k\pi\tau_{\mathrm{m}}}{2l} \tag{6}$$

3.2. Main circuit Specific Permeability Function

The addition of a magnetically conductive block to the primary of the motor (see Fig. 1) causes a change in the distribution of the specific permeability of the main magnetic circuit along the x-direction, which can be analyzed by using the specific permeability function [14], which is shown in the following equation:

$$\Lambda(x)=\frac{\mu_{0}}{\delta(x)} \tag{7}$$

where μ_0 is the air permeability; δ(x) is the electromagnetic air gap length function. Fig. 3 shows the specific permeability of the primary with the addition of the magnetic guide block.

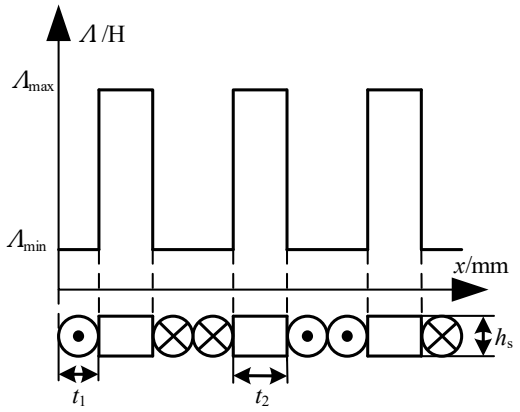

Figure 3. Specific magnetic permeability after primary

$$\Lambda(x)=\begin{cases}\Lambda_{\min} & -t_1+kT\le x<t_1+kT\\ \Lambda_{\max} & t_1+kT\le x<t_1+t_2+kT\end{cases} \tag{8}$$

where specific permeability $\Lambda_{max}=\mu_0/(h_m+g)$, g is the height of the air gap $\Lambda_{min}=\mu_0/(h_m+g+h_s/2)$, hs is the height of the coil edge, $T=2t_1+t_2$, and k=0,1,2, ...

A Fourier series expansion of the specific permeability function yields:

$$\Lambda(x)=\sum_{k=1}^{\infty}\Lambda_k\sin\frac{k\pi x}{l} \tag{9}$$

Which

$$\Lambda_k=\frac{2}{l}\int_0^l\Lambda(x)\sin\frac{k\pi x}{l}\mathrm{d}x \tag{10}$$

Substituting (8) into (10) yields.

$$\Lambda_k=\frac{4\Lambda_{\max}}{k\pi}\sin\frac{k\pi t_2}{2l}\sin\frac{(2k+1)k\pi T}{2l}+\frac{4\Lambda_{\min}}{k\pi}\sin\frac{k\pi t_1}{l}\sin\frac{k^2\pi T}{l} \tag{11}$$

Organizing is available:

$$\Lambda(x)=\sum_{k=1}^{\infty}\left(\frac{4\Lambda_{\max}}{k\pi}\sin\frac{k\pi t_2}{2l}\sin\frac{(2k+1)k\pi T}{2l}\right)\sin\frac{k\pi x}{l}+\sum_{k=1}^{\infty}\left(\frac{4\Lambda_{\min}}{k\pi}\sin\frac{k\pi t_1}{l}\sin\frac{k^2\pi T}{l}\right)\sin\frac{k\pi x}{l} \tag{12}$$

3.3. Air-Gap Flux Density

The air gap flux density can be solved analytically by the following equation

$$B(x)=F(x)\cdot\Lambda(x) \tag{13}$$

The relative positions of the primary and secondary of the motor at different moments are shown in Fig. 4.

According to the different relative positions of primary and secondary in Fig. 4, the no-load air-gap flux densities of the motor at different positions obtained by using the 2D finite element method and analytical method are shown in Fig. 5.

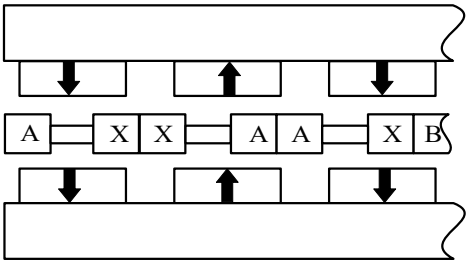

(a) Relative position 1

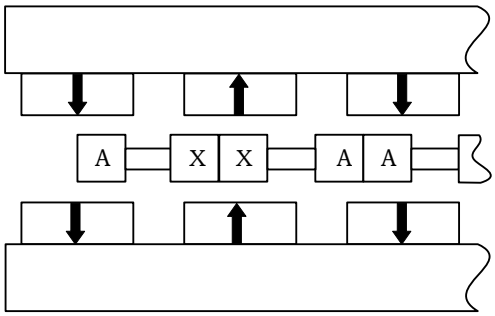

(b) Relative position 2

Figure 4. Relative positions of primary and secondary at different times

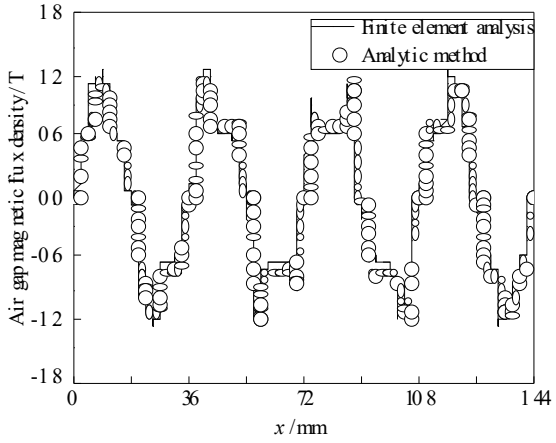

(a) Position 1

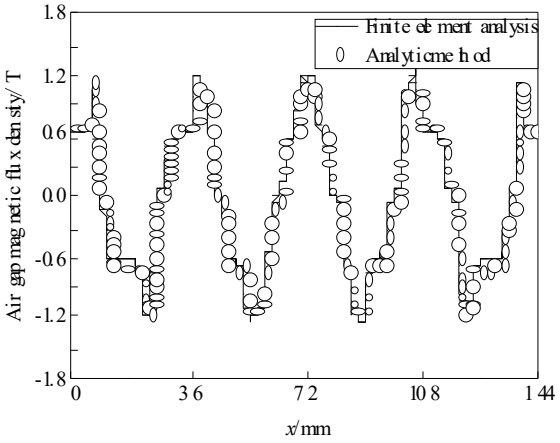

(b) Position 2

Figure 5. Air gap magnetic flux density corresponding to different relative positions

The results of the harmonic analysis of the air gap flux density are shown in Fig. 6.

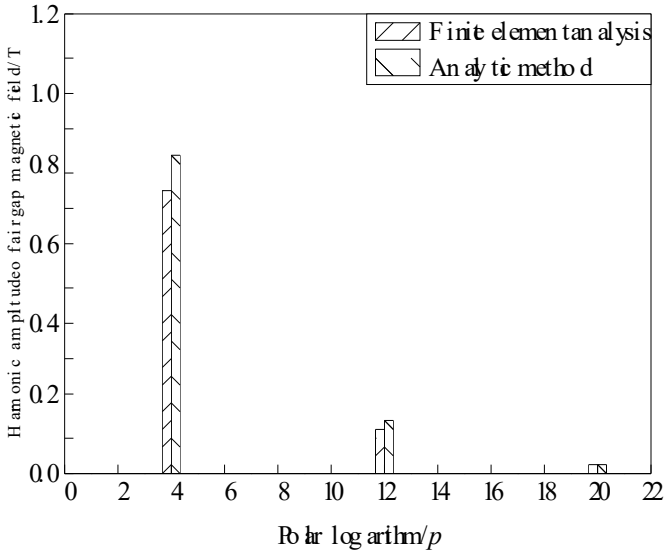

(a) Without iron core

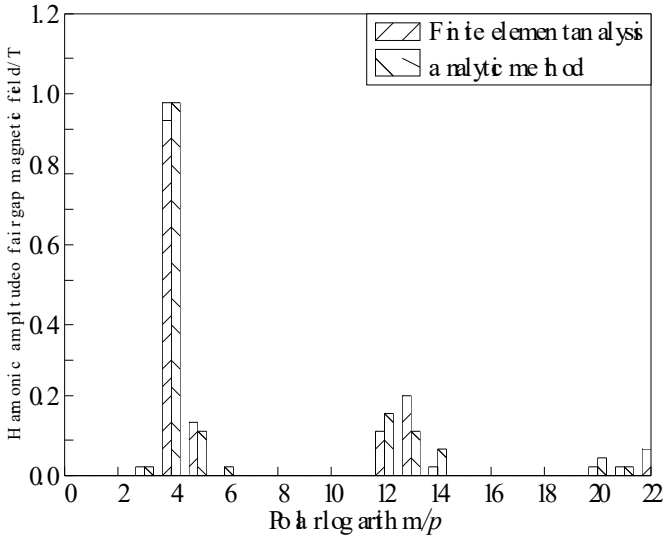

(b) With magnetic block

Figure 6. Harmonic analysis of air gap magnetic flux density

According to Fig. 6(a), it can be seen that the 4th harmonic flux density amplitude is the largest (0.75T) and plays a dominant role in the coreless linear motor. In addition, the 12th harmonic amplitude is higher at 0.1 T. From Fig. 6(b), it is seen that the 4th harmonic amplitude increases to 0.96 T and the 12th harmonic amplitude changes insignificantly.

Table 2. Motor thrust and thrust fluctuation

amagnetic guide	thrust /N	thrust fluctuation /%
exist	84.25	7.08
none	48.32	0.162

According to Table 2, it can be obtained that the electromagnetic thrust increases from 48.32N to 84.25N with the addition of the magnetic conductor block, which is an increase of 74.36% as compared to the air-core U-type motor. The thrust fluctuation increases from 0.162% to 7.08%. The

magnetizing block increases the fundamental wave component of the air gap magnetic field, so it increases the electromagnetic thrust. The magnetizing block also increases the high harmonic component of the air gap magnetic field and increases the thrust fluctuation. According to finite element the core loss of the motor can be obtained as shown in Table 3.

Table 3. Comparison of Core Losses

amagnetic guide	Iron core loss /W
exist	0.765123719
none	0.000754867

From Table 3, it is obvious that the addition of the magnetically conductive block has a significant effect on the iron core losses, and the difference between the two is quite large. Among them, the hysteresis loss plays a dominant role, while the eddy current loss in the iron consumption is relatively small and negligible. It is mainly due to the magnetizing ability of the magnetic conductor block, which leads to a higher magnetic flux density in the part of the magnetic conductor block in the primary, and thus the iron consumption is elevated.

4. OPTIMIZED DESIGN OF MOTORS

Output thrust F_{ave} and thrust fluctuation Frip are two important indexes to measure the performance of the motor, so the thrust and thrust fluctuation are selected as the optimization objectives in this paper. On the basis of using the same electrical load and the amount of permanent magnets, the permanent magnet pole arc coefficient α, coil side width t_1(mm), secondary back iron h(mm), radius of the chamfering radius of the magnetic guide block R(mm) and k_h(k_h is the ratio between the height of the magnetic guide block and the coil side) are selected as the optimization variables, and the height of the magnetic guide block is limited to not exceeding the height of the coil side, i.e., $k_h \leq 1$.

4.1. Influence of Different Parameters on the Motor

4.1.1. Effect of Chamfer Radius R on the Motor

Before optimization, it is first necessary to understand the specific impact of different parameters on the motor performance, so as to more accurately select the level value of Taguchi's method and lay a solid foundation for the optimization work.

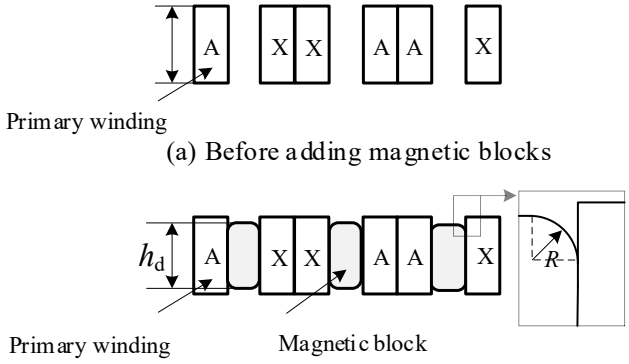

(a) Before adding magnetic blocks

(b) After adding magnetic blocks

Figure 7. Primary winding before and after adding magnetic blocks

As shown in Fig. 7, it is the comparison diagram before and after the primary is added to the conductor block, which has the effect of magnetization, and therefore can change the path of the magnetic flux in the space air gap; in order to reduce the oversaturation of the edge of the conductor block, which leads to the increase of iron consumption and local temperature rise, and at the same time to reduce the influence of thrust fluctuation, the conductor block is chamfered, as shown in Fig. 7(b).

Keeping the other parameters of the U-type linear motor unchanged, only the dimensional parameters of the chamfer radius R are changed, and the simulation is carried out using the two-dimensional finite element method, so as to obtain the relationship curves of thrust and thrust fluctuation with the chamfer radius R as shown in Fig. 8.

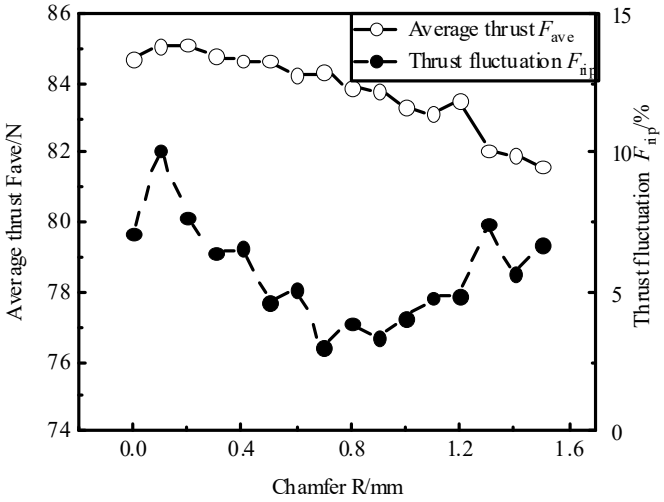

Figure 8. Effect of chamfer R on thrust and thrust fluctuation

The chamfer has a small effect on the motor thrust, and as the chamfer R increases, the overall average motor thrust decreases slightly because the increase of the chamfer R reduces the amount of the guide block to some extent, so it causes the motor thrust to decrease, however, the chamfer has a large effect on the fluctuation of the motor thrust, and the fluctuation of the motor thrust is minimized when R=0.7mm because the chamfer reduces the oversaturation of the edge of the guide block to some extent.

4.1.2. Influence of Conductive Block Coefficient k_h on Motors

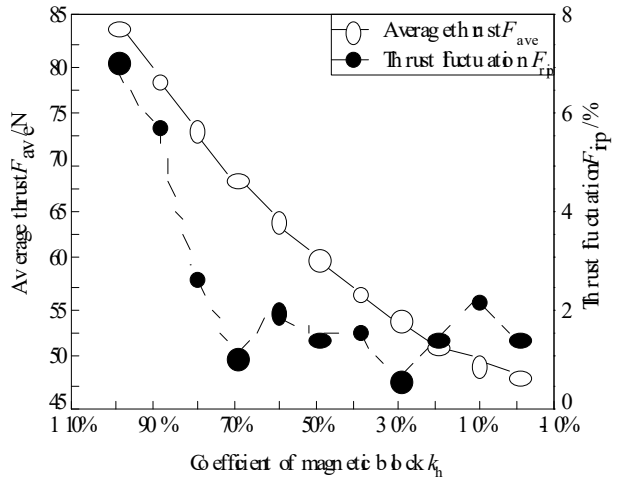

Figure 9. Influence of kh on thrust and thrust fluctuation

The size parameter of the height coefficient kh of the magnet-conducting block is adjusted while keeping the other key parameters stable and unchanged. Here, kh stands for the ratio of the height of the conductor block to the height of the primary winding, i.e., hd/hs. It serves as an important indicator of the amount of the conductor block, which has a significant impact on the motor performance.

According to Fig. 9, as the coefficient k_h of the magnetizing block gradually increases, the output thrust of the motor also shows an obvious growth trend. This is mainly because when k_h increases, the dosage of the magnetizing block increases accordingly, which in turn enhances the magnetizing ability of the primary winding. The increase in the magnetizing ability means that more magnetic chains interact effectively with the windings, thus increasing the thrust of the motor.

The increasing trend of thrust fluctuation is relatively flat when the coefficient k_h of the magnetizing block is less than 0.8. At this stage, the effect of k_h on the motor thrust is large, while the effect on the thrust fluctuation is not yet significant. In this paper, in order to better reflect the ability of the magnetizing block to enhance the motor thrust, therefore, k_h is chosen to be greater than 0.8.

4.1.3. Effect of Coil Side Width t_1 on the Motor

If the electrical load is kept constant, i.e., the coil area is kept constant, and the dimensional parameter of the coil side width t1 of the primary winding is adjusted, the coil side height hs will change accordingly. Different values of coil side width t1 are selected and analyzed as shown in Fig. 10.

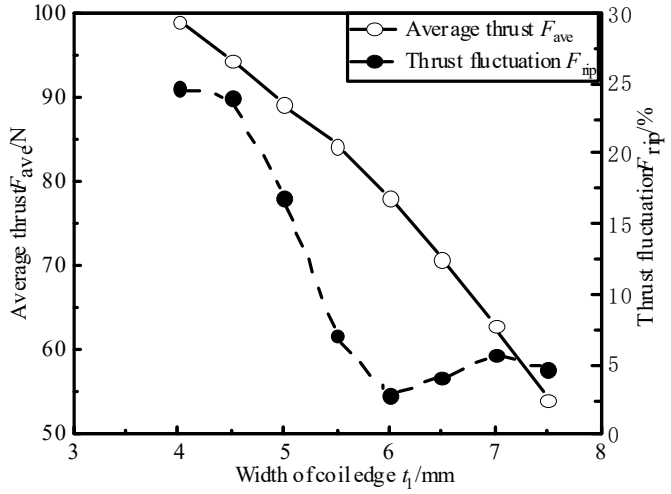

Figure 10. Effect of coil edge width t1 on motor performance

With the increase of the coil side width t_1, the output thrust shows a gradually decreasing trend, mainly because the increase of the coil side width t_1 will lead to the decrease of the coil height hs, which will make the width $t_2$of the magnetic guide block decrease, and the overall volume of the magnetic guide block become smaller. This weakens the magnetizing ability of the magnetic guide block and reduces the magnetic field strength, which leads to the reduction of the output thrust.

Although the reduction of the coil side width t_1 can enhance the magnetizing ability of the magnetic guide block, it will also exacerbate the imbalance of the magnetic flux in the space, leading to an increase in the fluctuation of the thrust. When the coil edge width t_1 reaches 6 mm, the thrust fluctuation reaches the minimum value, and at this time, the magnetizing ability and magnetic leakage ability reach an equilibrium state, which leads to the optimal performance of the motor.

In summary, if the thrust is kept large, i.e., k_h is larger than 0.8, the appropriate coil side width t_1 and chamfer R can still be selected to reduce the thrust fluctuation. However, to maintain a smaller thrust fluctuation, it is only necessary to reduce k_h below 0.8 at this point to meet the requirement.

4.2. Obtaining Optimization Objectives and Variables based on Taguchi Method

According to the influence of some parameters on the motor performance in the previous section, combined with the actual experience of engineering, it can be obtained that the optimization variables take the value range shown in Table 4:

Table 4. Value range of optimization variables

Optimization Variables	k_h	t_1/mm	α	R/mm	h/mm
Level 1	0.7	5.5	0.72	0.1	9
Level 2	0.8	6.0	0.77	0.3	10
Level 3	0.9	6.5	0.83	0.5	11
Level 4	1.0	7.0	0.88	0.7	12

The orthogonal test matrix established based on Taguchi's method for preliminary optimization of the motor. In order to analyze the effects of different optimization variables on the output thrust F_{ave} and thrust fluctuation F_{rip}, an average value analysis is performed on the finite element results of the orthogonal test matrix, and the average values of different optimization variables on the optimization targets at four level values are calculated, and the trends are shown in Fig. 11:

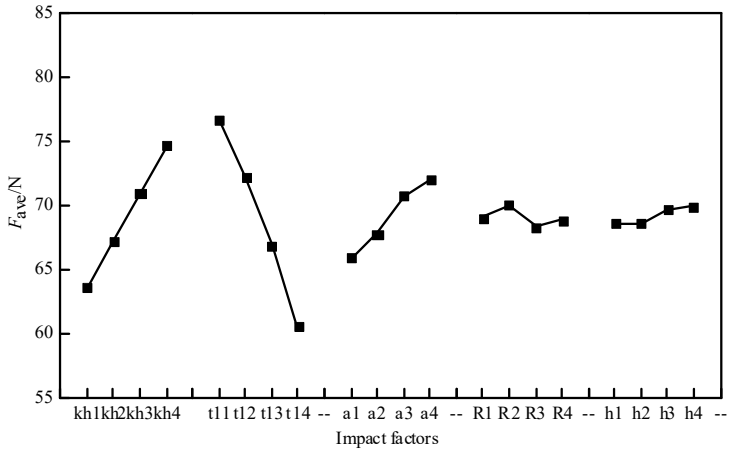

(a)Fave

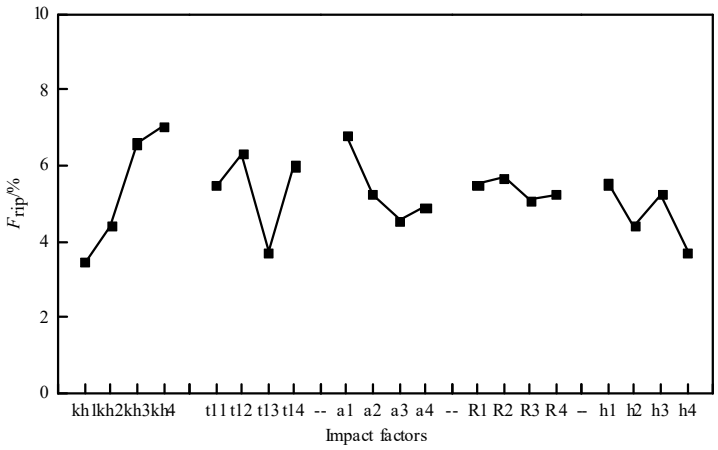

(b)Frip

Figure 11. Mean values of optimization objectives for different optimization variables at each factor level

From the simulation results in Fig. 11, it can be seen that each optimization variable cannot simultaneously satisfy the optimal combination of variables required for the two optimization objectives. According to the weight of the influence of each optimization variable on the optimization objective, the radius of the chamfering angle of the magnetic guide block R and the secondary back iron h have the smallest influence on the output thrust Fave, and have a larger influence on the thrust fluctuation Frip. Therefore, in order to reduce the thrust fluctuation, R_3 and h_4 are selected as the optimal levels, i.e., R takes the value of 0.5 mm and h takes the value of 12 mm.

4.3. Parameter Optimization based on Response Surface Method

Box-Behnken method is often used in response surfaces [15-16] for experimental design, and each variable factor takes three level values, which are the center value 0, upper limit 1, and lower limit -1 of the optimization interval of the design variables.According to the effect of different parameters on the motor in Taguchi's method, the ranges of values of the remaining three optimization variables were selected, which are shown in Table 5.

Table 5. Optimization variable level values

Optimization Variables	-1	0	1
t_1/mm	5.5	5.75	6
k_h	0.8	0.9	1
α	0.7	0.76	0.82

According to the experimental design principles of the Box-Behnken method, an orthogonal test matrix was established, as shown in Table 6.

Table 6. Orthogonal experimental matrix and experimental results

Test order	t_1/mm	k_h	α	F_{ave}/mm	F_{rip}/%
1	6	1	0.76	77.66135	3.54609
2	5.75	0.8	0.82	72.62376	2.157931
3	5.5	0.9	0.7	75.9472	8.27607
4	5.75	1	0.7	78.57107	5.978458
5	5.75	0.8	0.7	69.28039	1.977669
6	5.5	0.9	0.82	79.78921	7.539886
7	5.5	0.8	0.76	72.96935	2.548061
8	5.75	0.9	0.76	76.05757	5.555249
9	5.75	0.9	0.76	76.05757	5.555249
10	5.75	0.9	0.76	76.05757	5.555249
11	5.5	1	0.76	83.62828	5.372409
12	6	0.9	0.7	71.62382	5.816065
13	5.75	1	0.82	82.57132	6.164114
14	6	0.8	0.76	69.445	4.180469
15	6	0.9	0.82	75.11425	4.414208

The quadratic fitting formula between the optimization objective and the optimization variables is derived after response surface method analysis:

$$F_{\text{ave}} = 1632.9 - 394.21t_1 - 260.9k_{\text{h}} - 835.0\alpha + 35.774t_1^2 + 237.89k_{\text{h}}{}^2 + 575.4\alpha^2 - 24.43t_1 \cdot k_{\text{h}} - 5.86t_1 \cdot \alpha + 27.37k_{\text{h}} \cdot \alpha \tag{14}$$

$$F_{\text{rip}} = 1493 - 413t_1 + 211k_{\text{h}} - 1039\alpha + 39.1t_1^2 + 0.2k_{\text{h}}{}^2 + 723\alpha^2 - 34.6t_1 \cdot k_{\text{h}} - 11.1t_1 \cdot \alpha \tag{15}$$

4.4. Optimization Design of Electric Motor Based on Egret Swarm Optimization Algorithm

The egret flock optimization algorithm [17] is a heuristic algorithm that combines the predatory behavior of snowy egrets and great egrets, and consists of three main components: sit-and-wait strategy, proactive strategy, and discriminative conditions. It has better effectiveness and robustness compared to the Gray Wolf Optimization Algorithm and Harris Hawk Optimization Algorithm.

Objective function: the quadratic linear regression equations (14) and (15) equations derived from the response surface method are used as the optimization objective function.

The optimization variables and their value ranges are shown in Table 5.

The egret swarm optimization algorithm is used to optimize the multi-objective parameters, the population size is set to 100 and the maximum number of iterations is set to 500. the Pareto frontier is shown in Fig. 12.

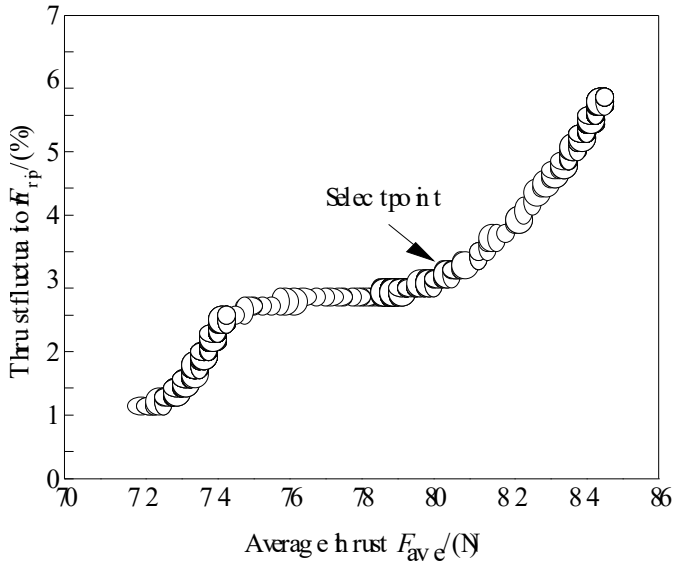

Figure 12. Pareto front with average thrust and thrust fluctuation as optimization objectives

As shown in Figure 12, the thrust fluctuation increases as the thrust increases. In practical application, the specific optimization scheme can be selected by taking into account the two objectives and compromising according to the engineering requirements. For example, the selection point is shown in Fig. 12, and on the right side of the selection point, the thrust fluctuation increases exponentially due to the increase of the polar arc coefficient α and the decrease of the coil side t_1. Near the left side of the picking point, there is no significant change in the thrust fluctuation as the thrust decreases. When the thrust force decreases below 74N, the motor thrust decreases steeply due to the decrease of the height coefficient k_{h} of the magnetic guide block. At the selection point, the motor output is moderate and the thrust fluctuation is small. Therefore, the selection point is the optimum point.

The design parameters before and after optimization are shown in Table 7.After optimization by the multi-objective egret swarm optimization algorithm, the thrust is slightly reduced and the thrust fluctuation is significantly reduced.

Table 7. Comparison of optimized design parameters

parameters	pre-optimization	post-optimization
α	0.78	0.785
t_1/mm	5.5	5.70
k_h	1.0	1.0
F_{ave}/mm	84.25	80.17
F_{rip}/%	7.08	3.57

The finite element simulation results are shown in Fig. 13. The average thrust of the motor after optimization is 82.02 N, and the thrust fluctuation is 3.45%, which is basically consistent with the results of the Beluga swarm optimization, which verifies that the Beluga swarm optimization algorithm has a significant effect on the multi-objective optimization design of the new U-type linear motor.

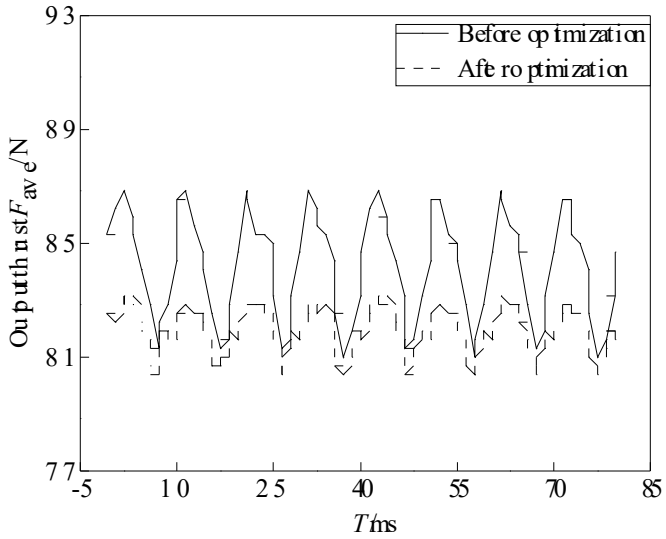

Figure 13. Comparison of motor thrust before and after optimization

5. SUMMARY

The new structure U-type motor proposed in this paper increases the fundamental wave component of the air gap magnetic field by adding a magnetic guide block in the primary, solves the no-load magnetic field of the motor by using the magnetic potential function and specific permeability function, and the analytical analysis results are basically consistent with the finite element analysis results; combining the response surface method with the egret swarm optimization algorithm to realize the multi-objective optimization of the motor, so that the electromagnetic thrust is increased by 74.36%, and the thrust fluctuation is controlled at about 3.5%, and the motor has practical value.

REFERENCES

[1] Song Heshen, Wang Taihua, Xu Xiaozhuo. Design and optimization of permanent magnet linear motors for oilfield sealing [J]. Manufacturing Automation, 2022, 44 (01): 42-45.

[2] Hong Weilin, Xiao Shuhong, Li Rongjian. Research on Minimizing Positioning Force of Cylindrical Permanent Magnet Linear Motor [J]. Combination Machine Tool and Automation Processing Technology, 2023 (10): 96-99.

[3] Lu Qinfen, Cheng Chuanying, Ye Yunyue, et al. A study on the number of slot poles in a fractional slot permanent magnet linear motor [J]. Chinese Journal of Electrical Engineering, 2012,32 (36): 68-74+12.

[4] WU Lize, LU Qinfen. Design and Optimization of High Acceleration Bilateral Permanent Magnet Linear Motor [J]. Micromotor, 2022, 55 (06): 1-5.

[5] LIU Hengkun, ZHANG Xiao, MI Zhu. Analysis of traction and normal force of hollow and Halbach permanent magnet linear synchronous motors [J]. Journal of National University of Defense Technology, 2012,34 (03): 94-97.

[6] Li B, Zhang J, Li Z A, et al. Research on Thrust Fluctuation of Linear Motor with Trapezoidal Halbach Pole[C]//2021 International Conference on Computer Network, Electronic and Automation (ICCNEA). China: IEEE,2021:303-309.

[7] WANG Guanghuang, DU Yumei, ZHANG Ruihua, et al. Structural optimization of medium speed maglev coreless permanent magnet linear synchronous motor [J]. Journal of Motor and Control, 2023,27 (05): 46-55.

[8] MIAO Zhongcui, SU Yi, ZHANG Lei, et al. Characteristics analysis and optimization design of trapezoidal Halbach alternating pole coreless permanent magnet synchronous linear motor [J/OL].Journal of Motor and Control:1-13.[2023-11-30]. http://kns.cnki.net/kcms/detail/23.1408.tm.20230531.1357.040.html.

[9] BODUROGLU A , DEMIR Y, CUMHUR B, et al. A Novel Track Structure of Double-Sided Linear PM Synchronous Motor for Low Cost and High Force Density Applications [J]. IEEE Transactions on Magnetics, 2021, 57(2) :1-5.

[10] YANG Xiong, ZHANG Fengge, WANG Xiuping. Analysis of electromagnetic characteristics of primary permanent magnet linear motor for rail transit [J]. Electrical Engineering, 2018,13(05): 1-7.

[11] Lan Yipeng, Liu Xin. Research on Control Strategy of Linear Motor Magnetic Suspension System for Feed Platform [J]. Combination Machine Tool and Automation Processing Technology, 2019 (08): 105-108.

[12] JIAO Y, YAO Z Y, HU Z X, et al. Optimum structural design of the miniature u-shape linear ultrasonic motor [C]//2011 Symposium on Piezoelectricity Acoustic Waves and Device Applications (SPAWDA). China: IEEE, 2011:80-83.

[13] MIRZAEI M, ABDOLLAHI S E, VAHEDI A. Permanent Magnet DC Linear Motor for Aircraft Electromagnetic Launcher [C] //2008 14th Symposium on Electromagnetic Launch Technology (SELT). Canada: IEEE,2008:1-6.

[14] PANG Gucai, DENG Zhiquan, ZHANG Zhongming. Analytical calculation of no-load air gap magnetic field in surface mounted permanent magnet motors based on improved generalized magnetic circuit method [J]. Journal of Electrical Engineering Technology, 2019, 34 (22): 4623-4633.

[15] SHANGUAN Xuanfeng, JIANG Siyuan, ZHOU Jingle. Design algorithm and multi-objective optimization of double squirrel cage permanent magnet induction motor [J]. Journal of Coal Industry, 2017,42 (S2): 611-618.

[16] HUANG H L, ZHANG J, ZHANG C. Multi-objective optimization design of U-PMVLM based on response surface method[C]// 2023 IEEE 18th Conference on Industrial Electronics and Applications (ICIEA), China: IEEE, 2023: 992-997.

[17] Chen Z Y, ADAM F, Li S, et al. Egret Swarm Optimization Algorithm: An Evolutionary Computation Approach for Model Free Optimization [J]. Biomimetics,2022,7(4):144.